



Heat transport in confined strongly coupled two-dimensional dust clusters

Giedrius Kudelis, Hauke Thomsen, and Michael Bonitz

Citation: [Phys. Plasmas](#) **20**, 073701 (2013); doi: 10.1063/1.4813244

View online: <http://dx.doi.org/10.1063/1.4813244>

View Table of Contents: <http://pop.aip.org/resource/1/PHPAEN/v20/i7>

Published by the [AIP Publishing LLC](#).

Additional information on Phys. Plasmas

Journal Homepage: <http://pop.aip.org/>

Journal Information: http://pop.aip.org/about/about_the_journal

Top downloads: http://pop.aip.org/features/most_downloaded

Information for Authors: <http://pop.aip.org/authors>

ADVERTISEMENT

An advertisement banner for AIP Advances. The top part features the 'AIP Advances' logo, which includes the text 'AIP Advances' in a green font and a series of orange and yellow circles of varying sizes arranged in an arc. Below the logo, the text 'Special Topic Section:' is written in white on a dark blue background, followed by 'PHYSICS OF CANCER' in large, bold, white capital letters. At the bottom, the text 'Why cancer? Why physics?' is written in a light green font, and a blue button with the text 'View Articles Now' is positioned to the right.

AIP Advances

Special Topic Section:
PHYSICS OF CANCER

Why cancer? Why physics? [View Articles Now](#)

Heat transport in confined strongly coupled two-dimensional dust clusters

Giedrius Kudelis,¹ Hauke Thomsen,^{2,a)} and Michael Bonitz^{2,b)}

¹University of Birmingham, Edgbaston, Birmingham B15 2TT, United Kingdom

²Institut für Theoretische Physik und Astrophysik, Christian-Albrechts-Universität zu Kiel, 24098 Kiel, Germany

(Received 17 April 2013; accepted 4 June 2013; published online 10 July 2013)

Dusty plasmas are a model system for studying strong correlation. The dust grains' size of a few micro-meters and their characteristic oscillation frequency of a few hertz allow for an investigation of many-particle effects on an "atomic" level. In this article, we model the heat transport through an axially confined 2D dust cluster from the center to the outside. The system behaves particularly interesting since heat is not only conducted within the dust component but also transferred to the neutral gas. Fitting the analytical solution to the radial temperature profiles obtained in molecular dynamics simulations allows to determine the heat conductivity k . The heat conductivity is found to be constant over a wide range of coupling strengths even including the phase transition from solid to liquid here, as it was also found in extended systems by Nosenko *et al.* [Phys. Rev. Lett. **100**, 025003 (2008)]. © 2013 AIP Publishing LLC. [<http://dx.doi.org/10.1063/1.4813244>]

I. INTRODUCTION

Strongly correlated systems are of high interest in modern physics. Strong correlations can emerge at very different physical regimes. In dusty plasmas, the high particle charge is responsible for the strong correlations, while ions in traps or laser plasmas can be strongly correlated due to low temperatures or the small particle distances (high density), respectively.^{1,2}

Besides static properties, experiments and molecular dynamics simulations have recently also provided insight to the dynamic properties. Particle transport (diffusion) is well investigated.^{3,4} Also, the heat transport is an important property that was experimentally investigated in extended systems.^{5,6} One question is how the strong correlations affect the transport properties.

In this article, we investigate the heat transport in a finite 2D dust cluster in an experiment-oriented simulation. After a brief presentation of the system model and the simulation technique in Sec. II, we present simulation results for different parameters in Sec. III. The analysis focuses on the temperature of the dust particles' random motion and the radial temperature profiles under different heating conditions. These profiles are compared to the solution of the stationary heat transport equation for the 2D cluster in Sec. III A, which allows to derive the thermal conductivity k under certain assumptions. Finally, we discuss the results for k and the dependence of k on heating power, equilibrium coupling strength, screening parameter, and friction in Sec. IV.

II. EXPERIMENTAL SETUP AND SIMULATION MODEL

2D dust clusters are usually realized by using a lower electrode with a cavity. The plasma sheath which contains the dust grains then reflects the shape of the cavity. This shape allows for a horizontal confinement of the dust. A

convenient way to investigate the heat transport is to heat the dust component in a restricted area. The laser manipulation technique^{7,8} is well suited for this purpose. Several randomly moving laser spots accelerate dust particles in different directions due to the momentum transfer by the radiation pressure. A spatially inhomogeneous heating is achieved by restriction of the area that is scanned by laser beams.

The unheated N -particle system is described by the Hamiltonian

$$H = \sum_{i=1}^N \frac{\mathbf{p}_i^2}{2m} + \sum_{i=1}^N \frac{m\omega^2}{2} \mathbf{r}_i^2 + \sum_{i<j} \frac{Q^2}{4\pi\epsilon_0 r_{ij}} e^{-r_{ij}/\lambda_D}, \quad (1)$$

where $r_{ij} = |\mathbf{r}_j - \mathbf{r}_i|$ is the pair distance and λ_D is the Debye length. The first term describes the classical kinetic energy of the dust grains. The confinement energy is also given by summation over all single particles in the second term. The trap frequency ω is basically set by the shape of the cavity in the lower electrode. Finally, the total interaction energy is given by summation over all $\frac{N(N-1)}{2}$ Yukawa-type pair interactions. This model assumes that all particles are equal in mass m and charge Q . Wake effects that occur in streaming plasmas, e.g., Refs. 9 and 10 can be neglected here, since we concentrate on a single layer of particles. The horizontal interaction is then adequately described by a Debye (Yukawa) potential.¹¹ This Hamiltonian is transformed to a dimensionless form by introducing $t_0 = 1/\omega$, $l_0 = \left(\frac{Q^2}{4\pi\epsilon_0 m\omega^2}\right)^{1/3}$ and $E_0 = \left(\frac{Q^4 m\omega^2}{(4\pi\epsilon_0)^2}\right)^{1/3}$ as units for time, length and energy. The Debye screening is then characterized by the screening parameter $\kappa = l_0/\lambda_D$. The length l_0 is the typical scale for the interparticle distance. In the case of two Coulomb interacting particles in the trap, their equilibrium distance is exactly $d_{2\text{part.}} = \sqrt[3]{2} \cdot l_0$. For more particles the distance changes by a factor of order unity.

While the dust component is treated exactly, electrons, ions, and neutral are treated statistically in the Langevin

^{a)}thomsen@theo-physik.uni-kiel.de

^{b)}bonitz@physik.uni-kiel.de

model. In this model, the amplitude of the stochastic force is expressed in terms of the friction coefficient γ between the dust particles and the neutral gas and the equilibrium temperature T_{eq} . T_{eq} and γ are input parameters to the simulation. We use Langevin molecular dynamics simulations¹² to propagate the equations of motion for the dust component and obtain the trajectories. The heating lasers are included as space and time dependent forces⁸

$$\mathbf{f}_l(\mathbf{r}, t) = \frac{P_0}{2\pi\sigma_x\sigma_y} \mathbf{e}_l \exp\left\{-\frac{(x-x_l(t))^2}{2\sigma_x^2} - \frac{(y-y_l(t))^2}{2\sigma_y^2}\right\}, \quad (2)$$

in this model where the index l counts the laser beam. The force amplitude is given by P_0 , whereas $\sigma_{x/y}$ describe the (in general) anisotropic spot profile, and \mathbf{e}_l is a unit vector in beam direction. We use a spot profile $\sigma_{\perp} = 0.1$ and $\sigma_{\parallel} = 0.5$ in units of l_0 which corresponds to a striking angle of $\alpha = 11.5^\circ$ between laser beam and levitation plane. Therefore, one spot can accelerate between one and a few dust grains simultaneously. The length scale for the interparticle spacing is of the order of millimeters under typical experimental conditions, $l_0 \approx 1\text{mm}$, and the particle diameter is typically several micrometers, $2r_p \approx 10\mu\text{m}$. Since each dust grain itself is small compared to the beam profile, the laser intensity is treated as constant across the particle's cross section. The choice of input power and spot size in an experiment is limited by the durability of the melamine grains. At high intensity, parts of the dust grains are evaporated causing a "rocket"-force.¹³ In the present simulations the intensities are chosen sufficiently low so that these effects are not relevant.

The trajectories of the moving spots in the levitation plane are denoted by $\mathbf{r}_l(t) = (x_l(t), y_l(t))$. We use two pairs of laser spots, one pair in x and one in y direction. The lasers of each pair accelerate the particles in opposite direction, thus the average total momentum transfer vanishes. The laser trajectories are generated randomly. The spot l moves across the levitation plane with velocity \mathbf{v}_l . When it reaches a border of the heated window, the motion is reverted in this direction and a new speed is randomly chosen within a given interval. This method was shown to allow for a controlled heating of the dust component without altering the properties of the plasma and the neutral gas.^{7,8}

We use the Coulomb coupling parameter $\Gamma = Q^2/(4\pi\epsilon_0 l_0 k_B T)$ (Refs. 14 and 15) as the ratio of typical interaction energy and thermal energy to characterize the coupling strength. While more accurate coupling parameters have been proposed for 2D Yukawa clusters, e.g., Ref. 16, for our purpose of investigating the heat conductivity over a broad range of coupling strengths, the present simple choice is sufficient. As characteristic particle distance, the unit length l_0 is used.

III. SIMULATION RESULTS

Figure 1 shows an example of the trajectories in a cluster with $N=200$ particles, with $\kappa = 1$ and $\Gamma_{\text{eq}} = 200$. The four laser spots move within a square with a side length

$a=1$ in units of l_0 . While the motion is restricted to a small region around the equilibrium position for particles at the cluster's edge, particles in the central region are less localized.

The trajectories in Fig. 1 show that the inner particles move larger distances within the same time than the outer ones. In order to quantify the associated temperature gradient, we calculate the radial temperature profile. Therefore, the simulation space is divided into concentric rings of width Δr . The width has to be chosen small enough to obtain a sufficient radial resolution and large enough to obtain a sufficient number of data points per ring. $\Delta r = 0.3$ in units of l_0 turned out as a proper choice. The temperature for the ring is calculated as $k_B T = m(\langle \mathbf{v}^2 \rangle - \langle \mathbf{v} \rangle^2)$ by taking the average over the whole simulation after an equilibration phase of typically $t_{\text{eq}} = 20\omega^{-1}$. The temperature profile reaches a steady state a few plasma periods ω^{-1} after "powering" the heating lasers in the simulation. The time resolved temperatures for three different radii are shown in Fig. 2. Since the dust cluster is trapped, the collective flow velocity $\langle \mathbf{v} \rangle$ vanishes. Figure 3 shows the velocity distributions of different rings from the center to the outside of the cluster. The distributions are Maxwellian for the inner rings as well as for the outer rings. The width of $p(v)$ is large in the center and decreases monotonically towards the cluster's border. That means, the temperature decreases with the radius, as expected.

A. Analytical model

In this section, we present an analytical model that can describe the radial dependence of the temperature. Our goal is to describe the dust temperature outside the central heated region. Therefore, we consider an incompressible fluid model and add the thermal coupling to the background gas with temperature T_{eq} in the heat transport equation^{17,18}

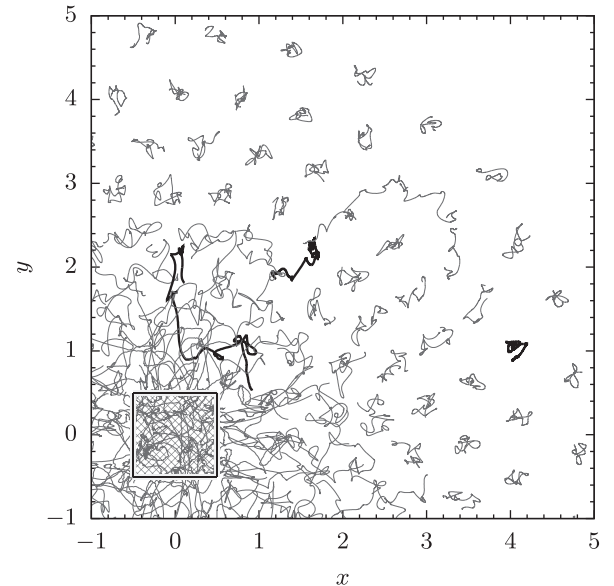


FIG. 1. Trajectories in the first quadrant of a heated Yukawa cluster during $\Delta t = 10l_0$. Each one arbitrary particle is highlighted in the central, middle, and outer region. The gray pattern around the origin indicates the array scanned by the laser spots. Parameters: particle number $N=200$, screening parameter $\kappa = 1$, equilibrium Coulomb coupling parameter $\Gamma_{\text{eq}} = 200$, friction parameter $\gamma = 0.5$, and heating power $P_0 = 90$.

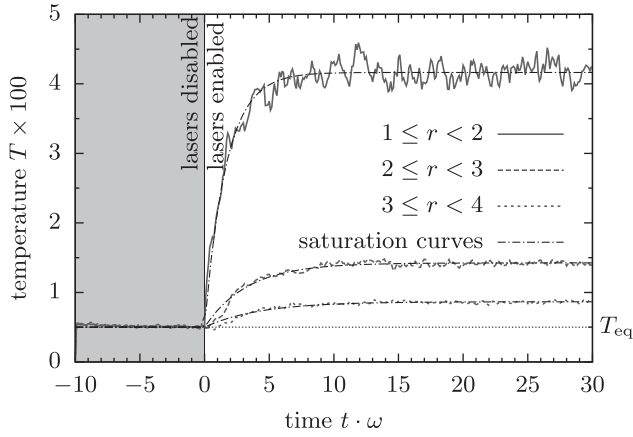


FIG. 2. Time evolution of the local temperature in the simulation for different radii. The lasers were “turned on” at $t=0$. While the temperature at the inside (top curve) saturates on a time scale $\tau = 1.7$, the relaxation is slower for the outer particles with $\tau = 4.3$. The temperatures were averaged over 40 independent simulations. Parameters: $N=200$, $\kappa = 1$, $\Gamma_{\text{eq}} = 200$, $\gamma = 0.5$, $P_0 = 50$. Prior to heating the cluster is in the crystal state.

$$c_p n \left(\frac{\partial T}{\partial t} + \mathbf{v} \nabla T \right) = \text{div}(k \nabla T) + S_v - 2\gamma n (T - T_{\text{eq}}), \quad (3)$$

where n is the average density, c_p is the specific heat, and \mathbf{v} is the flow velocity.⁶ The left-hand side of Eq. (3) represents the (convective) time derivative of the temperature. The right-hand side contains the thermal conduction and the shear heating as function of the spatial derivative of the velocity vector

$$S_v = \frac{\eta}{2} \left(\frac{\partial v_i}{\partial x_k} + \frac{\partial v_k}{\partial x_i} \right)^2, \quad (4)$$

where the indices i and k take values 1, 2 in two dimensions, and the squaring implies summation over i and k . The last term describes the losses to the neutral gas. If we wanted to describe the central region where the laser heating takes place, we would have to introduce another source term.

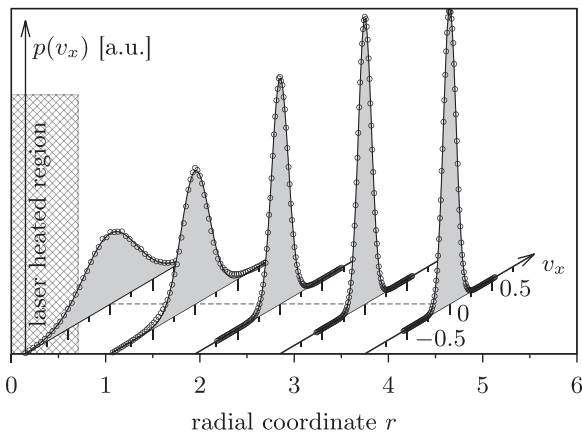


FIG. 3. Velocity distribution $p(v_x)$ of particles within concentric rings ($N=200$, moderate heating power $P_0 = 40$, equilibrium coupling strength $\Gamma_{\text{eq}} = 200$). The data points are well fit by Gaussians (filled curves) with decreasing width $\sigma_r(r) = \sqrt{k_B T(r)/m}$. The velocity distribution in y -direction $p(v_y)$ coincides with $p(v_x)$ and is not shown. The heated area is indicated by the gray pattern.

When the dust cluster is considered sufficiently long after equilibration, the temperature profile is constant and the partial time derivative $\frac{\partial T}{\partial t}$ vanishes. The *stationary* heat transport equation then reads¹⁸

$$c_p n \mathbf{v} \cdot \nabla T k_B = \text{div}(k \nabla T) - 2\gamma n (T - T_{\text{eq}}) k_B + S_v. \quad (5)$$

While the equilibrium temperature T_{eq} and the friction coefficient γ are input parameters to the simulation, the heat conductivity k is unknown. We further neglect the convective heat transport on the left side and heat input by viscous conversion of energy from a shear flow S_v since no shear flow is observed in the simulation data. We check the validity of the assumptions later by comparing the temperature profiles in the simulations with the analytic solution. The reduced heat transport equation then reads

$$\text{div}(k \nabla T) = 2\gamma n k_B (T - T_{\text{eq}}). \quad (6)$$

Due to the symmetry, we expect the temperature to depend on the radial coordinate r only, and rewrite Eq. (6) in polar coordinates as

$$\frac{1}{r} \frac{d}{dr} \left(r k \frac{dT}{dr} \right) = 2\gamma n k_B (T - T_{\text{eq}}). \quad (7)$$

Let us assume for a moment that losses to the neutral gas can be neglected ($\gamma = 0$) and the heat conductivity k is independent of r . Then, the solution of Eq. (7) is a logarithmic temperature profile, $T(r) = c_1 \ln(r/r_0)$, with the integration constants r_0 and c_1 . However, as shown in Fig. 4, this solution (cf. the dashed line) is unable to reproduce the temperature profiles from the simulations (symbols). The temperature in the simulations initially decays much faster than the logarithmic profile. Moreover, for larger radii the logarithmic solution continues to decay even below the gas temperature, while we expect the system to be always warmer than the surrounding gas due to heating applied. Hence, we conclude that consideration of losses to the neutral gas by

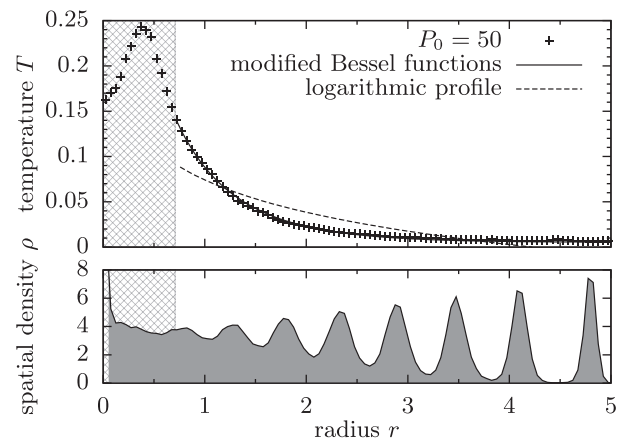


FIG. 4. The simulation data (symbols in upper plot, $N=200$, $\kappa = 1$, $T_{\text{eq}} = 0.005$, $\gamma = 0.5$) are fit by both a logarithmic temperature profile $T(r) = c_1 \ln(r/r_0)$ and by modified Bessel functions, Eq. (8). The latter fits the data well while the former solution does not. The central region was excluded from the fits since the power input by the lasers takes place in this region. The spatial density (lower plot) is almost constant in the central region where most of the heat loss to the neutral gas takes place.

friction is crucial for a correct treatment of the spatial heat distribution. These losses are responsible for the faster radial decay of the temperature.

The general solution of Eq. (7) with the heat conductivity k still assumed to be independent of r is readily found and given by modified Bessel functions of first kind I_0 and second kind K_0

$$T - T_{\text{eq}} = AK_0(\sqrt{b}r) + BI_0(\sqrt{b}r), \quad (8)$$

$$\text{with } b = \frac{2\gamma n k_B}{k}. \quad (9)$$

Since the dust cluster has a finite radial extension R , no heat can be transferred further outside. A heat flow equal to zero at $r = R$ is ensured in the solution, when the temperature gradient vanishes. When Eq. (8) is differentiated, we find the second coefficient, $B = AK_1(\sqrt{b}R)/I_1(\sqrt{b}R)$.

The solution Eq. (8) then has two remaining free parameters A and b which depend on the details of the laser heating, in particular, the heating power (see below). Since the heating is not included in Eq. (7) we determine these parameters by fitting the function to the simulation data. The central region where this input takes place is excluded from the fit. While the amplitude A is connected to the total power input, the thermal conductivity k is contained in b . The total heat that is transferred to the neutral gas outside the heated region (R_i) is calculated by integration of $dP_{\text{heat}} = 2n\gamma k_B(T - T_{\text{eq}})dA$,

$$\begin{aligned} P_{\text{heat}} &= 2\pi \int_{R_i}^R dr r 2n\gamma k_B [T(r) - T_{\text{eq}}] \\ &= 4\pi n\gamma k_B \frac{A \cdot R_i}{\sqrt{b}} \\ &\quad \times \left\{ K_1(\sqrt{b}R_i) - I_1(\sqrt{b}R_i) \frac{K_1(\sqrt{b}R)}{I_1(\sqrt{b}R)} \right\}. \end{aligned} \quad (10)$$

Since the $B/A = K_1(\sqrt{b}R)/I_1(\sqrt{b}R)$ decays fast, the second term can be neglected for clusters that are not too small. The ratio is $B/A < 2 \cdot 10^{-5}$, for $\sqrt{b}R \geq 5$, while it is of the order of 1 at the inner radius with $\sqrt{b}R \approx 1$. The total heating power is, therefore, approximately given by

$$P_{\text{heat}} \approx 4\pi n\gamma \frac{A \cdot R_i}{\sqrt{b}} K_1(\sqrt{b}R_i). \quad (11)$$

The dependence on the inner radius R_i remains, since Eq. (11) is the heat loss to the neutral gas outside the central region only and hence, depends on the size of this excluded region.

Equation (10) establishes the relation of the two free parameters with the given input power P_0 . Since the radial temperature profile is well fit by the modified Bessel functions as solution of Eq. (7), see Figs. 4–6, we conclude that Eq. (7) correctly captures the physics.

B. Influence of equilibrium temperature T_{eq} and heating power P_0

In this section, we investigate the influence of the gas temperature T_{eq} and the laser power P_0 on the thermal

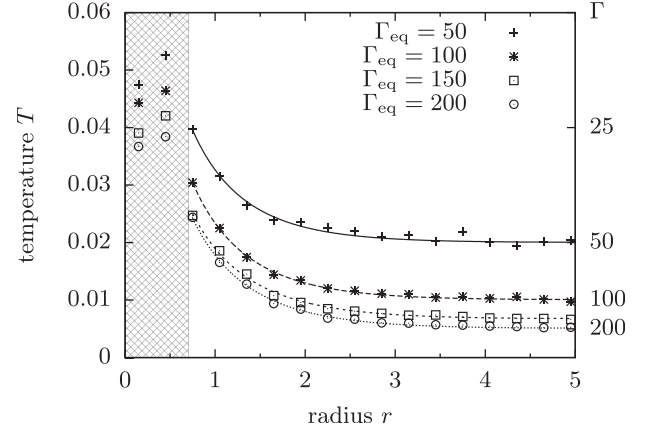


FIG. 5. Simulation data (symbols) and fits by modified Bessel functions (lines) for different equilibrium temperatures and constant heating power $P_0 = 20$. The central region was always excluded. On the right axis, the temperature is translated into a local coupling parameter (averaging over the shells²⁰).

conductivity. A central question is, whether the heat conduction changes during the transition between the solid-like and liquid-like regimes. The melting point of a macroscopic 2D Coulomb ($\kappa = 0$) system is well known as $\Gamma = 137$ (Ref. 14), whereas for $\kappa = 1$ it is around $\Gamma \approx 180$.¹⁴ Due to finite size effects, we do not expect a sharp transition temperature but a transition range¹⁹ and choose the analyzed range of Γ accordingly.

As a first parameter scan, the equilibrium temperature of the Langevin thermostat is varied at constant heating power. The radial temperature profiles for four different values of T_{eq} are shown in Fig. 5. We used a comparatively small laser power for this plot, since the background temperatures are of the same order of magnitude as the central temperatures in that case. The temperature approaches T_{eq} towards the cluster boundary in all four simulations. Varying T_{eq} has also an effect on the temperature of the heated particles in the center. The temperature is increased by an increase of T_{eq} . This observation is not surprising, since heat input by collisions with the neutral gas (i.e., via the stochastic force) and heat input by the laser force add up. While the amplitude of the

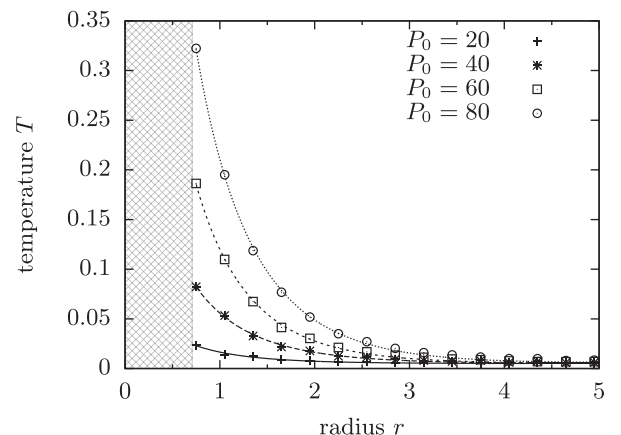


FIG. 6. Simulation data (points) and fits by modified Bessel functions (lines) for different heating powers. The central region was always excluded. The equilibrium temperatures corresponds to $\Gamma_{\text{eq}} = 200$ in all cases.

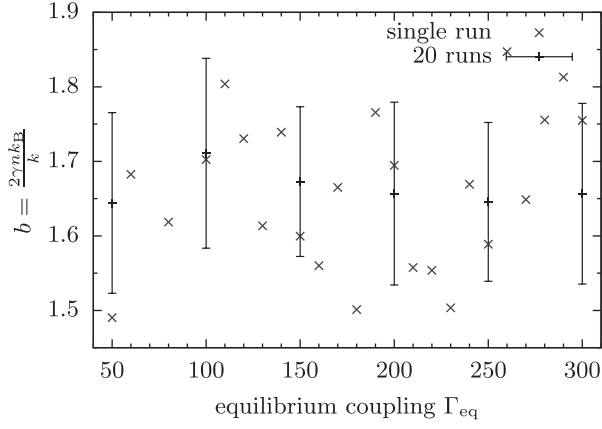


FIG. 7. Values of the parameter b for different equilibrium temperatures Γ_{eq} . Each symbol represents a single simulation. The error bars show the variance of the single estimates of b . Parameters: $N=200$, $\kappa=1$, $\gamma=0.5$, $P_0=100$.

temperature increases with T_{eq} , interestingly, the parameter b remains constant. However, the dispersion of the single measurements is large as seen in Fig. 7. In order to estimate the statistical variation of b , we performed a series of 20 simulations, for each value $\Gamma_{\text{eq}} = 50, \dots, 300$. Each run uses the same parameters but different random numbers and initial particle positions. Mean value and standard deviation of b are also plotted in Fig. 8. Within the simulation accuracy, we find that $b = 1.57 \pm 0.01$ ($P_0 = 50$) and $b = 1.66 \pm 0.01$ ($P_0 = 100$) is constant when T_{eq} is varied. A series of 20 simulations was also performed with moderate coupling $\Gamma_{\text{eq}} = 1$ and $P_0 = 100$. The density profile becomes wide at the cluster boundary but is only changed weakly at the inside where most of the heat is transferred and lost to the neutral gas. With that, the result for $b = 1.5 \pm 0.7$ indicates the essential independence of thermal conductivity on the coupling parameter over a wide parameter range of a strongly coupled plasma.

In a second parameter scan, the laser power is varied while the equilibrium temperature is fixed corresponding to

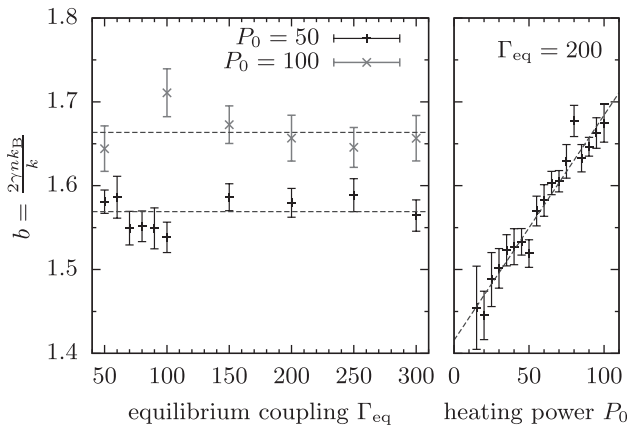


FIG. 8. Values of the parameter b for different equilibrium temperatures of the Langevin thermostat (left) and for different heating powers (right). Each symbol represents the average from 20 independent simulations with the variance of this average as error bar. The horizontal dashed lines indicate the mean value of $\bar{b} = 1.57 \pm 0.01$ for $P_0 = 50$ and $\bar{b} = 1.66 \pm 0.01$ for $P_0 = 100$ in dimensionless units. The power dependence is well reproduced by a linear fit, $b = b_0 + m \cdot P_0$, with $b_0 = 1.42 \pm 0.01$ and $m = 2.68 \pm 0.18 \times 10^{-3}$. Simulation parameters: $N=200$, $\kappa=1$, $\gamma=0.5$.

$\Gamma_{\text{eq}} = 200$. The temperature profiles for four exemplary powers are shown in Fig. 6. The higher power input results in an increased temperature in the cluster inside. For small powers, the equilibrium temperature is reached at the cluster's outer radius. For higher powers, the temperature of the outer particles is about twice as high as the equilibrium temperature. Interestingly, the parameter b shows a linear dependence on the heating power within the accuracy of the estimation, see right side of Fig. 8.

IV. DISCUSSION OF THE RESULTS

In this section, we give an interpretation of the simulation results and compare them with experimental results for bulk systems. The parameter b , as introduced in Eq. (8), has the dimension of an inverse length squared. Hence, $L = 1/\sqrt{b}$ can be interpreted as *characteristic length* for the heat transport. For arguments greater than 2, the modified Bessel function K_1 is well approximated by an exponential decay, and the temperature difference $T(r) - T_{\text{eq}}$ is found to drop by a factor ≈ 2.5 each L in radial direction. The mean value of $\bar{b} = 1.66$ from the simulations for different equilibrium temperatures, Fig. 8, translates into $L = 0.78$, meaning that L is close to the average interparticle distance.

Another quantity which is often calculated in experiments^{6,21,22} is the thermal diffusivity $\chi = k/(nc_p)$, where c_p is the specific heat (heat capacity per particle). To estimate c_p the excitations of the strongly correlated dust cluster can be approximated by the $2N$ normal modes, where one (the rotation of the whole cluster) does not contribute: $c_p \approx (2N - 1)/N \approx 2$. With this we obtain a thermal diffusivity of

$$\chi = \frac{k}{nc_p} = \frac{2\gamma nk_B}{bnc_p} = \frac{\gamma k_B}{b} \approx 4.4 \text{ mm}^2/\text{s}. \quad (12)$$

The conversion from dimensionless units into SI units was done for melamine particles with $d_p = 6 \mu\text{m}$ diameter, a charge of $Q = 10\,000e_0$, a trap frequency $\omega = 5.5 \text{ s}^{-1}$ and a friction frequency $\gamma = \omega/2$ as typical plasma parameters. This result is in reasonable agreement with experimental findings of $\chi \approx 9 \text{ mm}^2/\text{s}$ and $\chi_{\text{tr}} \approx 30 \text{ mm}^2/\text{s}$ (transversal), $\chi_1 \approx 50 \text{ mm}^2/\text{s}$ (longitudinal), for 2D complex plasmas,^{6,22} and $\chi \approx 1 \text{ mm}^2/\text{s}$, in a liquid 3D complex plasma,²¹ where the different friction values give rise to the largest uncertainty.

In the present dissipative system, the stationary temperature profile and the decay length L are governed by the competition of two processes: temperature transport within the dust system (characterized by k) and energy loss to the neutral gas (proportional to γ). In fact, using Eq. (9) the decay length can be rewritten as

$$\frac{L}{(nk_B)^{1/2}} = \left(\frac{k}{2\gamma}\right)^{1/2}, \quad (13)$$

where both 2γ and k can be considered as relevant energy exchange collision frequencies. An increase of the intra-dust energy transport (i.e., increase of k) increases the length L , in

contrast, increased dissipation (γ) causes a temperature drop over a shorter distance. This picture of two competing processes assumes that both are independent. This is, in fact, the case for the data presented in the simulations above, where an average dust-neutral gas friction frequency $\gamma = 0.5$ (in units of ω) was used which is typical for many experiments.

At the same time, 2D experiments can access a rather broad range of friction parameters, depending on the used gas pressure. Also, from the theory side, it is interesting to study the dust particle behavior in the different limits of weak and strong dissipation. We, therefore, performed a series of additional simulations where the dust-neutral gas friction was varied between $\gamma = 0.1$ and $\gamma = 1.0$, at constant other parameters. The results are shown in Fig. 9. The top figure indicates that the decay parameter b monotonically increases with γ as one would expect from (Eq. (13)) since $b = L^{-2}$. If the dust-dust heat transport and heat loss to the neutral gas would be independent of each other this increase of b would be linear in γ . This is more easily studied by analyzing directly the dependence of the heat conductivity k on γ which is shown in Fig. 9(b). In fact, k remains almost constant for a strongly dissipative plasma, $\gamma \geq 0.4$, and this result is observed independent of the heating power.

Interestingly, for weak dissipation, $\gamma \lesssim 0.4$, the picture changes qualitatively. The heat conductivity k increases when γ is being reduced, see Fig. 9(b). One possible reason

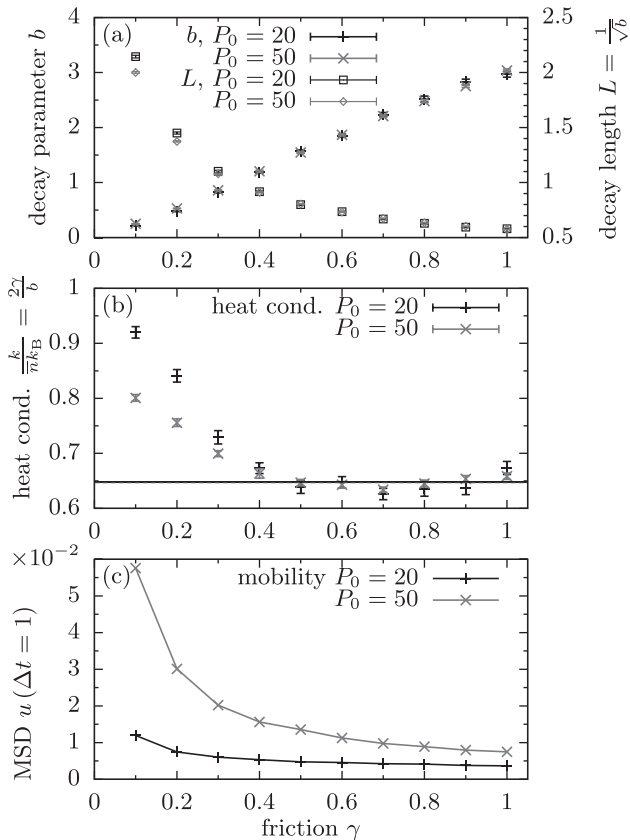


FIG. 9. (a) Dependence of the fitted decay parameter b (growing curves) and the corresponding decay length L (decreasing curves) on the friction coefficient γ . (b) The heat conduction k appears constant at high γ while it increases when γ is being reduced, for $\gamma \lesssim 0.4$. (c) The mobility of the dust grains is characterized by the MSD, see text, at a time difference $\Delta t = 1$ in units of ω^{-1} .

for the increased heat conductivity at low friction γ is the increased mobility of the dust grains. To verify this hypothesis, we compute the mean square displacement (MSD)

$$u(\Delta t) = \langle (\mathbf{r}_i(t_0 + \Delta t) - \mathbf{r}_i(t_0))^2 \rangle_{i,t_0}, \quad (14)$$

at a time difference $\Delta t = 1$ (in units of ω^{-1} (Ref. 23)) where we averaged over the whole trajectory (over time point t_0) of all particles (i). The result is shown in Fig. 9(c) indicating that the mobility increases with decreasing γ . In case of high mobility, long-range particle motion can become important. Furthermore, equilibrium particle transport in a strongly correlated 2D plasma is known to exhibit anomalous diffusion,²⁴ at least for intermediate times that is strongly influenced by dissipation.²⁵ It may be expected that in the present externally driven system such effects will be of similar relevance and also manifest themselves in other transport quantities and in a coupling of different quantities. Obviously, this requires to go beyond the simple fluid model, Eq. (6).

In summary, we have shown that the radial heat transport in a confined strongly coupled 2D Yukawa cluster is well described by a fluid model over a wide parameter range. In this model, we obtained an analytical result for the radial temperature profile. Using this model, Langevin molecular dynamics results revealed that the heat conductivity is constant over the investigated broad temperature range that includes the transition region between liquid-like and solid-like clusters. A theoretical explanation based on a fluid theory that includes correlation effects,²⁶ as well as, shell formation^{26,27} is still missing as is a microscopic result for the heat conductivity of strongly correlated dust clusters. Furthermore, it would be of high interest to verify the present predictions in an experiment with laser heated dust clusters.

ACKNOWLEDGMENTS

This work was supported by the Deutsche Forschungsgemeinschaft via SFB-TR24 (projects A5 and A9), by the German Academic Exchange Service via the RISE program and a grant for computing time at the HLRN (grant shp00006).

¹A. Ivlev, H. Löwen, G. Morfill, and C. P. Royall, *Complex Plasmas and Colloidal Dispersions: Particle-Resolved Studies of Classical Liquids and Solids* (World Scientific, 2012).

²M. Bonitz, C. Henning, and D. Block, *Rep. Prog. Phys.* **73**, 066501 (2010).

³T. Ott and M. Bonitz, *Phys. Rev. Lett.* **103**, 195001 (2009).

⁴T. Ott and M. Bonitz, *Phys. Rev. Lett.* **107**, 135003 (2011).

⁵Y. Feng, J. Goree, and B. Liu, *Phys. Rev. E* **86**, 056403 (2012).

⁶V. Nosenko, S. Zhdanov, A. V. Ivlev, G. Morfill, J. Goree, and A. Piel, *Phys. Rev. Lett.* **100**, 025003 (2008).

⁷J. Schablinski, D. Block, A. Piel, A. Melzer, H. Thomsen, H. Kählert, and M. Bonitz, *Phys. Plasmas* **19**, 013705 (2012); A. Melzer *et al.*, *Contrib. Plasma Phys.* **52**, 795 (2012).

⁸H. Thomsen, H. Kählert, M. Bonitz, J. Schablinski, D. Block, A. Piel, and A. Melzer, *Phys. Plasmas* **19**, 023701 (2012).

⁹P. Ludwig, W. J. Miloch, H. Kählert, and M. Bonitz, *New J. Phys.* **14**, 053016 (2012).

¹⁰D. Block *et al.*, *Contrib. Plasma Phys.* **52**, 804 (2012).

¹¹A. Piel and A. Melzer, *Plasma Phys. Controlled Fusion* **44**, R1 (2002).

- ¹²R. Mannella, *Phys. Rev. E* **69**, 041107 (2004).
- ¹³V. Nosenko, A. V. Ivlev, and G. E. Morfill, *Phys. Plasmas* **17**, 123705 (2010).
- ¹⁴P. Hartmann, G. J. Kalman, Z. Donkó, and K. Kutasi, *Phys. Rev. E* **72**, 026409 (2005).
- ¹⁵F. M. Peeters and X. Wu, *Phys. Rev. A* **35**, 3109 (1987).
- ¹⁶T. Ott, M. Stanley, and M. Bonitz, *Phys. Plasmas* **18**, 063701 (2011).
- ¹⁷L. D. Landau and E. Lifschitz, *Course of Theoretical Physics VI, Fluid Mechanics*, 2nd ed. (Pergamon Press, Oxford, 1990).
- ¹⁸We added the Boltzmann constant k_B in Eq. (3) to allow temperatures in Kelvin. In the heat transport term, k_B is absorbed by the thermal conductivity k . Furthermore, we use the areal particle density n instead of the mass density ρ .
- ¹⁹S. Hamaguchi, R. T. Farouki, and D. H. E. Dubin, *Phys. Rev. E* **56**, 4671 (1997).
- ²⁰C. Henning, P. Ludwig, A. Filinov, A. Piel, and M. Bonitz, *Phys. Rev. E* **76**, 036404 (2007).
- ²¹V. E. Fortov, O. S. Vaulina, O. F. Petrov, M. N. Vasiliev, A. V. Gavrikov, I. A. Shakova, N. A. Vorona, Y. V. Khrustalyov, A. A. Manohin, and A. V. Chernyshev, *Phys. Rev. E* **75**, 026403 (2007).
- ²²S. Nunomura, D. Samsonov, S. Zhdanov, and G. Morfill, *Phys. Rev. Lett.* **95**, 025003 (2005).
- ²³The precise choice of the time Δt is not crucial. The only condition is that Δt exceeds the initial time where the motion of the particles is ballistic. A different choice does not alter the curves in Fig. 9(c) qualitatively, but leads to a rescaling of the y-axis.
- ²⁴T. Ott, M. Bonitz, and P. Hartmann, *Phys. Rev. Lett.* **103**, 099501 (2009).
- ²⁵T. Ott and M. Bonitz, *Contrib. Plasma Phys.* **49**, 760–764 (2009).
- ²⁶J. Wrighton, J. W. Dufty, H. Kählert, and M. Bonitz, *Phys. Rev. E* **80**, 066405 (2009).
- ²⁷J. Wrighton, H. Kählert, T. Ott, P. Ludwig, H. Thomsen, J. W. Dufty, and M. Bonitz, *Contrib. Plasma Phys.* **52**, 45 (2012).